Palaeogeography, Palaeoclimatology, Palaeoecology 628 (2023) 111756

Contents lists available at ScienceDirect

Palaeogeography, Palaeoclimatology, Palaeoecology

journal homepage: www.elsevier.com/locate/palaeo

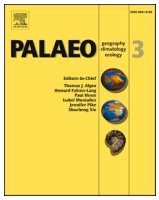

Carbonate uranium isotopes across Cretaceous OAE 2 in southern Mexico: New constraints on the global spread of marine anoxia and organic carbon burial

Joseph T. Kulenguski [a], Geoffrey J. Gilleaudeau [a,*], Alan J. Kaufman [b], Michael A. Kipp [c], François L.H. Tissot [c], Tyler J. Goepfert [d], Alan D. Pitts [e], Pietropaolo Pierantoni [e], Michael N. Evans [b], Maya Elrick [f]

[a] Department of Atmospheric, Oceanic, and Earth Sciences, George Mason University, Fairfax, VA 22030, USA
[b] Department of Geology and Earth System Science Interdisciplinary Center, University of Maryland, College Park, MD 20742, USA
[c] The Isotoparium, Division of Geological and Planetary Sciences, California Institute of Technology, Pasadena, CA 91125, USA
[d] School of Earth and Space Exploration, Arizona State University, Tempe, AZ 85281, USA
[e] University of Camerino, Geology Division, School of Sciences and Technology, 62032 Camerino, MC, Italy
[f] Department of Earth and Planetary Sciences, University of New Mexico, Albuquerque, NM 87131, USA

ARTICLE INFO

Editor: A Dickson

Keywords:
Oceanic Anoxic Event
Ocean deoxygenation
Uranium isotopes
Carbonates
Cretaceous

ABSTRACT

Oceanic anoxic events (OAEs) represent discrete intervals of decreased marine oxygen concentrations often associated with volcanism, enhanced organic carbon burial coupled with positive $\delta^{13}C$ excursions, and significant biotic turnover. Cretaceous OAE 2 (ca. 94 Mya) is especially notable for globally-distributed changes in calcareous invertebrate and plankton populations. While the presence of organic-rich facies is consistent with locally anoxic environments in many cases, determining the global extent of anoxia is more problematic. To address this issue, we investigate uranium isotope ($\delta^{238}U$) compositions of upper Cretaceous (Cenomanian-Turonian) open marine platform carbonates from southern Mexico as a proxy for global seawater redox conditions. These data are complementary to previous $\delta^{238}U$ studies across OAE 2 in both black shales and pelagic carbonates, which have yielded variable results that reflect both global redox and local depositional processes. In Morelos Formation carbonates, a significant and well-defined negative $\delta^{238}U$ excursion down to a nadir of −0.6‰ is recorded over an ~40 m interval. This is consistent with the expansion of marine anoxia, pointing to an areal extent of anoxic seawater of about 1–10% of the global seafloor (or ~5 to 50 times the modern value). Importantly, based on biostratigraphically-controlled estimates of sediment accumulation rates, the $\delta^{238}U$ anomaly precedes the $\delta^{13}C$ excursion by a median of ~45 to 51 kyr (95th percentile confidence interval, CI) or ~105 to 120 kyr (95th percentile CI) depending on how the onset of the $\delta^{238}U$ anomaly is estimated. These results, along with previously reported thallium isotope and trace metal data, suggest that anoxic expansion preceded carbon cycle perturbation. This observation further increases estimates of the duration of OAE 2, implying that widespread ocean anoxia may have lasted >900 kyr.

1. Introduction

The Mesozoic Era is known for greenhouse climate conditions, elevated atmospheric pCO_2, increased igneous activity, biotic turnover, and discrete periods of decreased marine oxygen concentrations known as oceanic anoxic events (OAEs). At least three Cretaceous OAEs are characterized by distinctive organic-rich facies (e.g., black shale or dark laminated limestone) and globally correlative positive $\delta^{13}C$ excursions preserved in both carbonate and organic matter (Jenkyns, 2010). These discrete events appear to be associated with enhanced volcanism, high pCO_2, and elevated temperatures, as well as an invigorated hydrological cycle, which stimulated primary productivity and marine anoxia (Takashima et al., 2006; Jenkyns, 2010; Pogge von Strandmann et al., 2013; DuVivier et al., 2014; Charbonnier et al., 2018; Chen et al., 2022a). These integrated environmental impacts resulted in significant extinction of marine biota. As such, OAEs provide a potential analogue

* Corresponding author.
E-mail address: ggilleau@gmu.edu (G.J. Gilleaudeau).

https://doi.org/10.1016/j.palaeo.2023.111756
Received 5 May 2023; Received in revised form 24 July 2023; Accepted 28 July 2023
Available online 30 July 2023

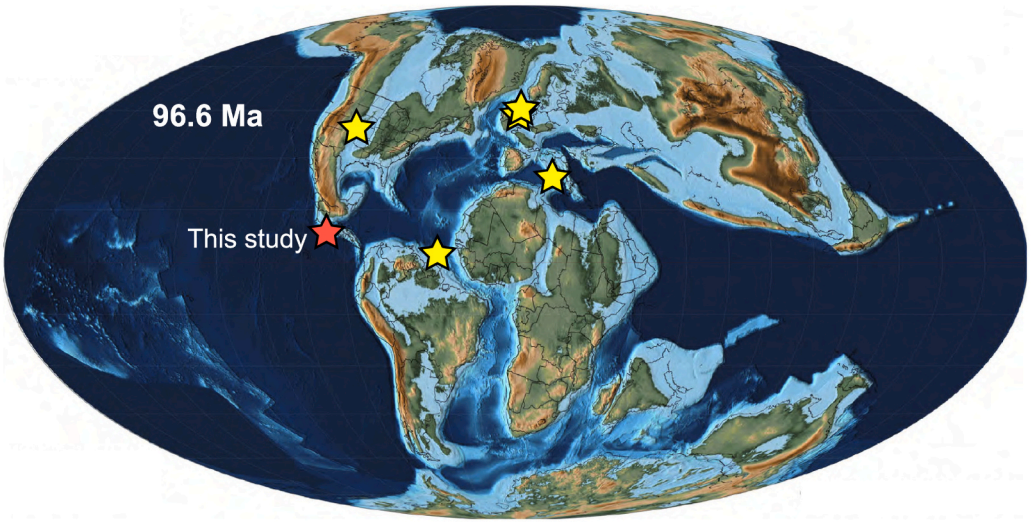

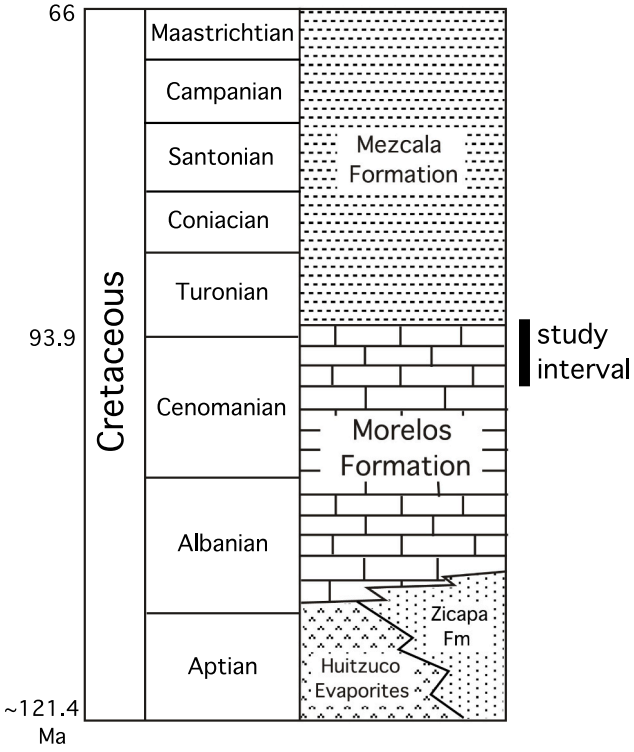

Fig. 1. (Top) Paleogeographic map for the Cenomanian (96.6 Ma) showing OAE 2 sites studied previously for $\delta^{238}U$ with yellow stars (Montoya-Pino et al., 2010; Clarkson et al., 2018; McDonald et al., 2022) and the Guerrero-Morelos platform studied here with a red star (map modified from Scotese, 2014). (Bottom) Generalized Cretaceous stratigraphy of the Guerrero-Morelos platform, with the study interval highlighted by the black bar on the right. (For interpretation of the references to colour in this figure legend, the reader is referred to the web version of this article.)

for the effects of anthropogenic climate change on ocean oxygen availability.

One such widely studied event is OAE 2, which coincides with the Cenomanian-Turonian boundary (~94 Mya), with prominent black shale and organic-rich limestone deposition in the Western Interior Seaway (WIS) of North America, across the Mediterranean region of modern Europe, and at many deep-sea sites across the Atlantic and Pacific oceans (e.g., Trabucho Alexandre et al., 2010; Jarvis et al., 2011; Lenniger et al., 2014; Lowery et al., 2017). These coeval deposits preserve large positive $\delta^{13}C$ excursions, indicating a global perturbation to the carbon cycle (Tsikos et al., 2004). Whereas the presence of organic-rich facies is often indicative of local anoxia, it is difficult to quantify its global extent during OAE 2 insofar as many seafloor deposits of this antiquity have been consumed by subduction. Constraining the area of anoxic seafloor during OAE 2 is important for understanding the consequences of this event on global biogeochemical cycles, marine nutrient balance (especially phosphorus availability; e.g., Handoh and Lenton, 2003), and ocean ecosystems.

Previous determinations of the extent of seafloor anoxia during OAE 2 have relied on sedimentological and paleontological data (e.g., Uchman et al., 2013), geochemical proxies for local redox conditions (Hetzel et al., 2009; Robinson et al., 2023), redox-sensitive isotope systems such as sulfur, molybdenum, thallium, and uranium (Adams et al., 2010; Montoya-Pino et al., 2010; Owens et al., 2013; Westermann et al., 2014;

Dickson et al., 2016; Gomes et al., 2016; Ostrander et al., 2017; Clarkson et al., 2018; Raven et al., 2019; McDonald et al., 2022), patterns of global trace metal drawdown (Hetzel et al., 2009; Westermann et al., 2014; Dickson et al., 2016; Owens et al., 2016), and model-data comparisons (Monteiro et al., 2012; Kipp and Tissot, 2022). Compared to the ~0.2% of seafloor covered by anoxic waters in the modern ocean (Veeh, 1967; Bertine and Turekian, 1973; Tissot and Dauphas, 2015), proposed estimates for OAE 2 have ranged widely from 1 to 2% (Montoya-Pino et al., 2010) to 21% (McDonald et al., 2022) of the global seafloor covered by anoxic waters, with other estimates suggesting that at least 50% of the ocean volume became anoxic (Monteiro et al., 2012). This wide range of variability is likely due to different sensitivities of different geochemical systems to the global spread of marine anoxia, as well as different parameters used in different modeling exercises and differences in the ability of various sedimentary archives (e.g., carbonate, black shale) to record and preserve this information.

One of the most promising, recently developed, and widely applied tools for global paleo-redox reconstruction is the uranium isotope ($\delta^{238}U$) composition of marine carbonate rocks (Lau et al., 2019; Zhang et al., 2020; Kendall, 2021). In this study, we focused on uranium isotopes applied to well-preserved carbonates spanning OAE 2 from the Guerrero-Morelos platform of southern Mexico (Fig. 1), which unlike previously studied samples, were deposited on an open margin away from any epeiric or restricted watermasses. We also present new carbon and oxygen isotope, as well as uranium concentration data from a pelagic carbonate section through OAE 2 in the Scaglia Bianca Formation, central Apennines, Italy. Uranium isotopes have emerged as a reliable proxy for the extent of anoxia in ancient oceans, rooted in the premise that removal of isotopically heavy ^{238}U to anoxic sediments (to a larger degree than other oceanic sinks for U) exerts a first-order control on the $\delta^{238}U$ value of seawater (Weyer et al., 2008; Tissot and Dauphas, 2015), with relative changes in seawater $\delta^{238}U$ recorded in marine carbonates under certain conditions (Romaniello et al., 2013; Chen et al., 2018; Tissot et al., 2018). We compare our results to published $\delta^{238}U$ profiles from pelagic, epeiric sea carbonates spanning OAE 2 in Europe (Clarkson et al., 2018) and the Western Interior Seaway of North America (McDonald et al., 2022), as well as an open ocean black shale succession from Demerara Rise (Montoya-Pino et al., 2010). Our $\delta^{238}U$ profile from the Morelos Formation reveals a prominent negative excursion that provides new constraints on the extent and duration of global ocean anoxia across OAE 2, as well as its impact on organic carbon burial.

2. Background

2.1. Geology of the Guerrero-Morelos platform

During the Cretaceous, southern Mexico was located at ~23–28° N paleolatitude and a broad, westward-facing carbonate platform accumulated ~2 km of peritidal to deep subtidal carbonates overlain by open-marine pelagic facies (Hernandez-Romano et al., 1997; Aguilera-Franco and Hernandez-Romano, 2004; Fig. 1). The studied Barranca el Tigre (BT) succession is composed of ~600 m of medium to thick-bedded, bioturbated shallow-water skeletal carbonates (Morelos Formation) immediately overlain by thinner-bedded, pelagic carbonate and fine siliciclastics of the Mezcala Formation. At the study site, the Morelos Formation is dominated by shallow to deep subtidal peloidal to skeletal wackestone and packstone containing abundant benthic foraminifera, echinoderms, rudist bivalves, gastropods, green algae, ostracods, and rare oncolites, as well as some evidence for high-energy storm deposits. The abundance of body and trace fossils in the Morelos Formation suggests accumulation under well-oxygenated conditions. The position of the Cenomanian-Turonian boundary in this shallow-water succession was identified by correlating distinctive trends in the BT $\delta^{13}C$ record to the biostratigraphically well-dated global $\delta^{13}C$ profile (Elrick et al., 2009).

2.2. Uranium isotope systematics

Naturally occurring U primarily exists as the ^{238}U and ^{235}U isotopes, and in seawater it is found primarily in the insoluble and particle-reactive U(IV) and soluble U(VI) oxidation states. The soluble U(VI) forms stable uranyl carbonate complexes in seawater and, as a result, has a residence time (~400–500 kyr; Ku et al., 1977) that is much longer than the ocean mixing time (1–2 kyr), making U concentrations and isotopes well-mixed across the global ocean (at 35 psu [practical salinity units]: $[U]_{sw}$ = 3.2 ng/g, Owens et al., 2011; $\delta^{238}U_{sw} = -0.379 \pm 0.023‰$, Kipp et al., 2022). The largest magnitude of U isotope fractionation in the oceans occurs during the burial of U in sediments under anoxic conditions, with most modern studies focusing on euxinic (anoxic + sulfidic) environments (Weyer et al., 2008; Holmden et al., 2015; Rolison et al., 2017; Zhang et al., 2020). This fractionation is driven by the reduction of U(VI) to U(IV), which enriches U(IV) in ^{238}U and leaves dissolved U(VI) enriched in ^{235}U (Bigeleisen, 1996; Brown et al., 2018). Consequently, sediments deposited under euxinic conditions record $\delta^{238}U$ values ~0.4 to 1.2‰ heavier than seawater (Lau et al., 2019; Kendall, 2021). Recent data suggest that substantially less fractionation (<0.4‰) occurs under anoxic, iron-rich (Cole et al., 2020) or suboxic conditions (Bruggmann et al., 2022). Thus, $\delta^{238}U$ is increasingly considered a proxy specifically for marine euxinia (Gilleaudeau et al., 2019; Bruggmann et al., 2022). Lau et al. (2022) also found a relationship between isotopic fractionation during U removal to anoxic sediments and hydrographic factors such as primary productivity and basin restriction, suggesting that non-euxinic environments can also impact the global U isotope mass balance. Despite these complications, we suggest that the size of the anoxic sink for U in the oceans is the primary control on seawater $\delta^{238}U$ values, and thus in this study, use our $\delta^{238}U$ data to model the broader extent of marine anoxia across OAE 2. Insofar as an increase in the extent of oceanic anoxia drives the removal of ^{238}U, periods of expanded anoxia will leave residual seawater with lower $\delta^{238}U$ values. This relationship allows seawater $\delta^{238}U$ values to be related to the global extent of marine anoxia, with many previous studies aimed at quantifying this relationship (e.g., Montoya-Pino et al., 2010; Gilleaudeau et al., 2019; Kendall, 2021; Kipp and Tissot, 2022).

Analysis of Bahamian Pleistocene-Holocene carbonates reveals that measured $\delta^{238}U$ values typically record an offset of ~0.2 to 0.4‰ from seawater caused by accumulation of isotopically heavy authigenic U(IV) under sulfidic pore water conditions, although this offset can vary from ~0 to 0.6‰ under different diagenetic conditions (Chen et al., 2018; Tissot et al., 2018) and has been suggested to complicate reconstruction of seawater $\delta^{238}U$ across OAE 2 (McDonald et al., 2022). In this study, we followed the recommendation of recent work (e.g., Kipp and Tissot, 2022; McDonald et al., 2022) in exploring multiple approaches to correct for diagenetic isotopic offsets. Specifically, we used both a uniform 0.3‰ offset (e.g., Romaniello et al., 2013) and a variable $0.23 \pm 0.15‰$ offset (Tissot et al., 2018) to correct our shallow-water carbonate data and infer $\delta^{238}U_{sw}$ in our modeling exercise. We note that uncertainty in this offset can obscure chemostratigraphic trends (see Discussion). $\delta^{238}U$ in marine carbonates as a reliable redox proxy is supported by results from seven Permo-Triassic marine carbonate successions from different ocean basins and diagenetic settings which each record a negative $\delta^{238}U$ excursion across the extinction interval of roughly the same magnitude, although some records show more variability than others (Brennecka et al., 2011; Lau et al., 2016; Elrick et al., 2017; Zhang et al., 2018).

3. Methods

We analyzed 34 samples for U abundance, spanning 75 m of the Morelos Formations from the BT section. We also analyzed 19 samples for U abundance from the mid-Cretaceous Scaglia Bianca Formation collected at the Bottaccione Gorge near Gubbio, central Apennines, Italy. Uranium abundances were measured in the pelagic Scaglia Bianca Formation as a comparison to coeval platform carbonates of the Morelos

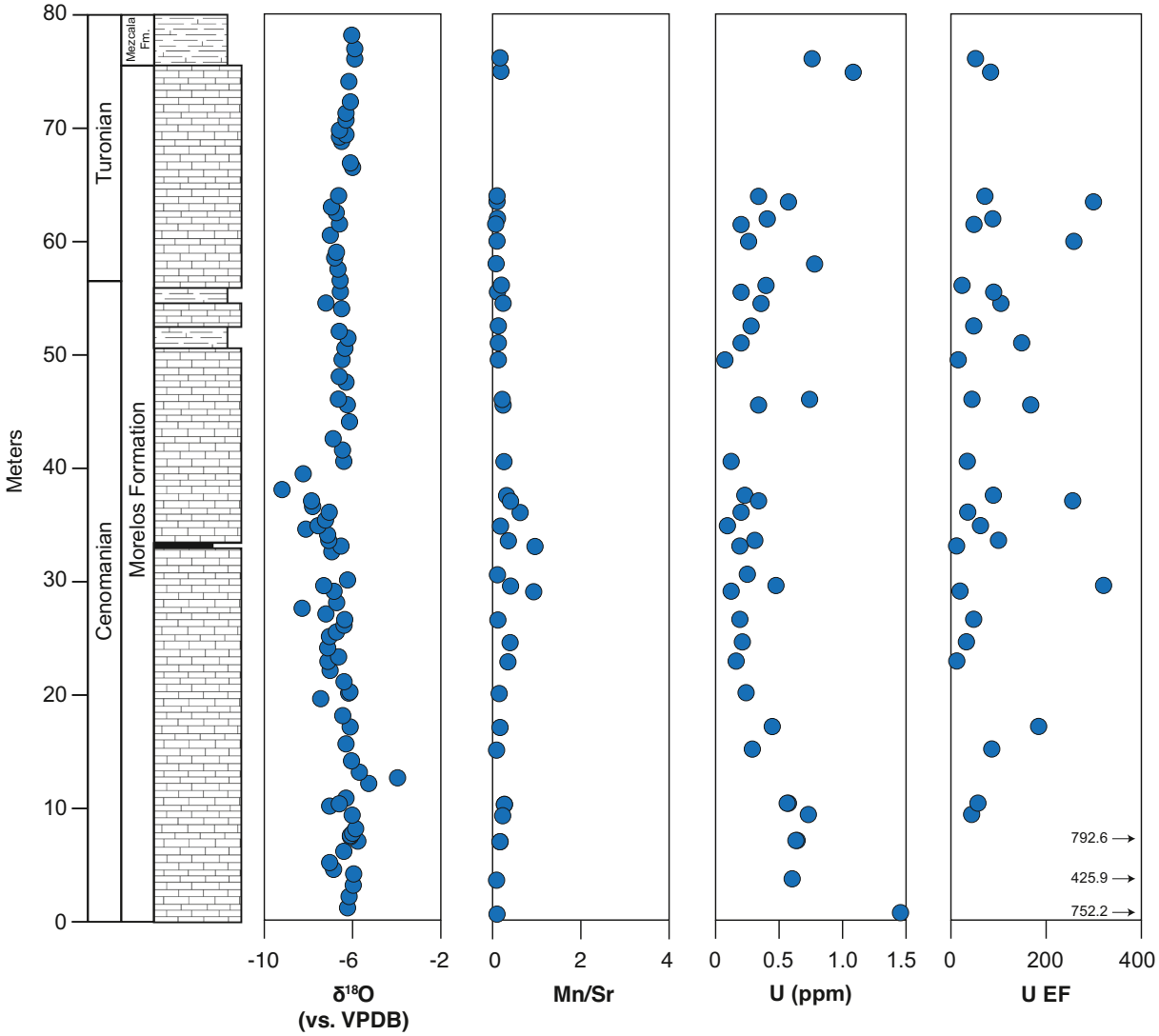

Fig. 2. Stratigraphic plots of important geochemical variables through the studied Barranca el Tigre (BT) section. Note that $\delta^{18}O$ values are relatively invariant near −6‰, with the exception of a discrete interval with values down to −9‰ between 35 and 38 m. All $\delta^{18}O$ values (with the exception of two data points) are between −5.9 and −8.3‰. Mn/Sr ratios—which are used as a diagenetic indicator—are <1 in all samples. Both of these variables indicate a high degree of preservation of primary geochemical signatures. Uranium concentrations range from 0.06 to 1.47 ppm, which is a typical range for Phanerozoic platform carbonates (e.g., Jost et al., 2017; Elrick et al., 2022). Note that U EFs are substantially elevated above 1, indicating a strong component of authigenic U from seawater in these platform carbonates. $\delta^{18}O$ data from Elrick et al. (2009).

Formation. Samples from both Italy (collected for this study) and Mexico (Elrick et al., 2009) were chipped using a plastic-wrapped rock hammer with any weathered surfaces removed. Chips were then crushed to a fine powder at George Mason University in an agate ball mill. ~1.5 g of powdered sample was treated with 40 mL of trace-metal-grade 1 M HNO_3 in metal-free centrifuge tubes. Samples were subject to Vortex mixing and left to sit for 24 h at room temperature. Treated samples were centrifuged and the supernatant separated. Approximately 200 μL of supernatant was removed, diluted to ~200 ppm Ca with 2% HNO_3, and analyzed for U concentrations using an Element 2 ICP-MS at the University of Maryland.

A full suite of major, trace, and rare-earth element concentrations was also measured on all samples on a Thermo iCAP™ quadrupole ICP-MS at Arizona State University. Typical precision is reported based on repeated analysis of simultaneously run standards, and in this study, relative percent s.d. was better than 6% for all reported elements. For samples from the Morelos Formation, the remainder of the solution was dried and used for $\delta^{238}U$ analysis. $\delta^{238}U$ composition was determined using a $^{236}U/^{233}U$ double-spike (IRMM-3636; Vergbruggen et al., 2008) to correct for instrumental mass fractionation. Before column chemistry, 0.8 mL of a 10.7 ppb double-spike solution was added per 500 ng of U to achieve a U_{spike}/U_{sample} ratio of ~1.7% (Weyer et al., 2008; Gilleaudeau et al., 2019). Samples were treated with reverse aqua regia (3:1 HNO_3:HCl), H_2O_2, concentrated HNO_3, and ultimately re-dissolved in 3 M HNO_3. Uranium was separated from matrix elements through ion exchange chromatography using UTEVA resin. Uranium separation was performed twice to ensure removal of all matrix elements. The separated U was dissolved in 2% HNO_3 to a concentration of 50 ppb and analyzed at Arizona State University on a Thermo Scientific Neptune multi-collector ICP-MS. The standard solution (CRM 145) was analyzed every two samples, with these values used to normalize sample $\delta^{238}U$ values via standard-sample bracketing. A second standard solution (CRM 129a) was analyzed after every ten analyses to ensure analytical reproducibility. The median $\delta^{238}U$ value we measured for CRM 129a is -1.68 ± 0.11‰ ($n = 17$, 2 s.d.). Precision of sample $\delta^{238}U$ values is reported as 2 s.d. of replicate measurements of the same sample solutions. Average precision for the sample set is ±0.06‰.

$\delta^{13}C$ and $\delta^{18}O$ data for the Morelos Formation come from Elrick et al.

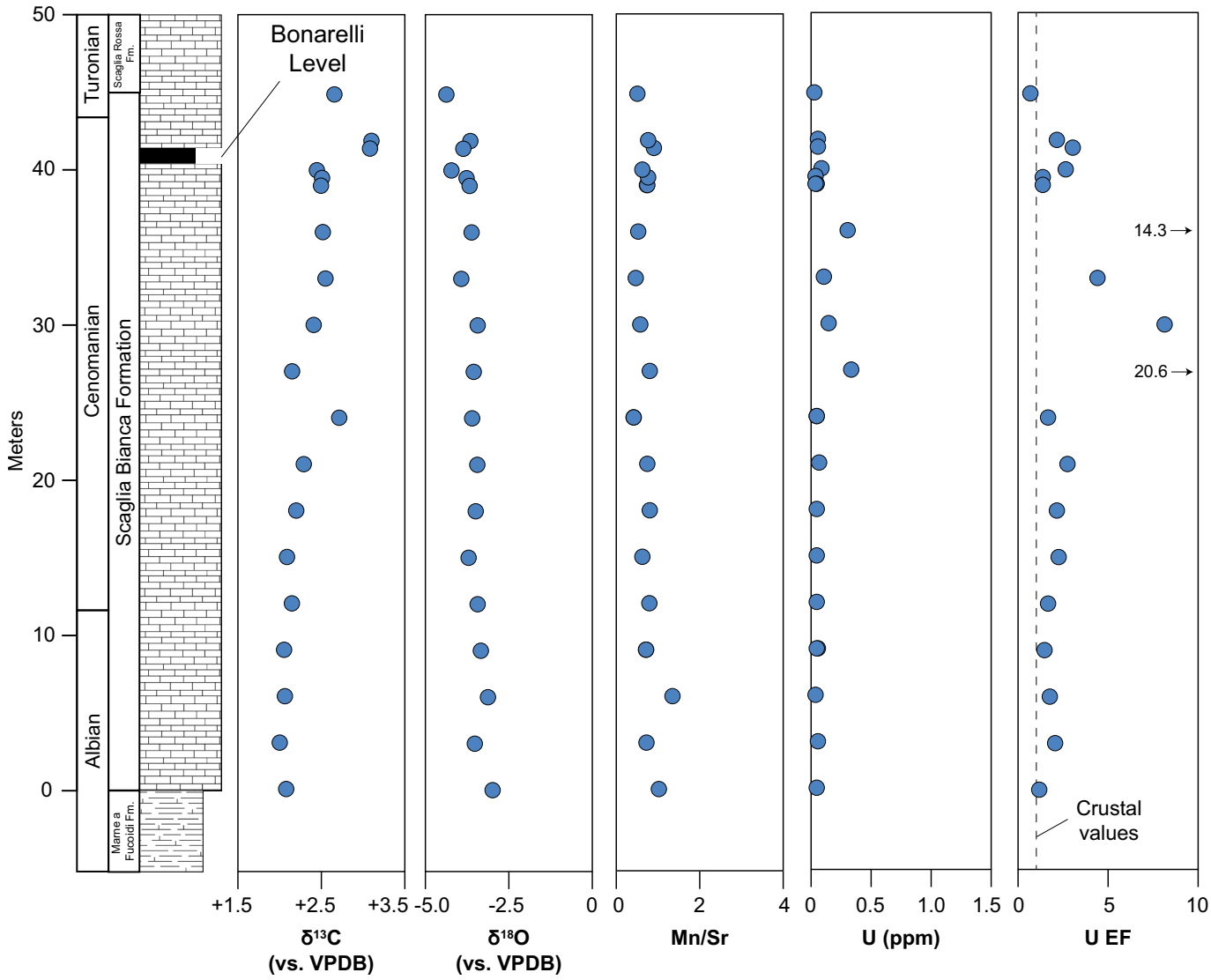

Fig. 3. Stratigraphic plots of important geochemical variables through the studied Scaglia Bianca Formation, measured and collected at the Bottaccione Gorge near Gubbio, central Apennines, Italy. Note the prominent black shale level at ~40 m. This is the Bonarelli Level, which is the local stratigraphic expression of OAE 2. Note the low U abundances through this pelagic carbonate section, as well as U EF values that show minimal enrichment of samples in authigenic U about a crustal baseline.

(2009), but in this study, we generated $\delta^{13}C$ and $\delta^{18}O$ data for the 19 samples from the Scaglia Bianca Formation. These data were collected from 100 μg splits of powdered samples by continuous flow isotope ratio mass spectrometry (CF-IRMS) on a GV Multiflow peripheral coupled to an Elementar Isoprime at the University of Maryland. Samples were flushed with 99.999% He in sealed exetainers, then manually acidified, reacted for 1 h, and sequentially analyzed, with working standard carbonates analyzed in replicate every 12 samples, relative to a 99.999% CO_2 monitoring gas. Data are reported on sample amplitudes within the range 2–8 nA, corrected for sequential drift, amplitude, and mean biases based on a working standard calibrated on the IAEA-CO1 – L-SVEC scale for both $\delta^{13}C$ and $\delta^{18}O$ (JTB assigned values: $\delta^{13}C = +1.78‰$, $\delta^{18}O = -8.71‰$), and reported relative to the V-PDB reference ratio (Evans et al., 2016). Blank amplitudes before and after sample analysis were < 0.1 nA, and system linearity over the amplitude range 1–10 nA was observed to be <0.02‰/nA in both $\delta^{13}C$ and $\delta^{18}O$ before batch analyses. External precision of analysis, based on replicate corrected working standard $\delta^{13}C$ and $\delta^{18}O$ analyses ($n = 28$; amplitude range 3–8 nA), were 0.05‰ and 0.11‰, respectively.

4. Results

Uranium concentrations in platform carbonates of the Morelos Formation range from 0.06 to 1.47 ppm with a median value of 0.31 ppm (Fig. 2), whereas U concentrations in pelagic carbonates of the Scaglia Bianca Formation range from 0.02 to 0.33 ppm with a median value of 0.04 ppm (Fig. 3). Platform carbonate U abundances are thus nearly tenfold higher than their pelagic counterparts, consistent with low initial U concentrations in previously reported pelagic calcite sediments (Clarkson et al., 2020, 2021; Chen et al., 2022b). We calculated the U enrichment factor (EF) based on sample U/Al ratios compared to the upper continental crust (Rudnick and Gao, 2003), which provides an estimate of the relative contributions of authigenic U in carbonate and detrital U in clays in the sample solution, acknowledging that some leaching of U from clays is possible during a 1 M HNO_3 dissolution. In the Morelos Formation, U EFs range from ~8 to 817, with values >20 in all but four samples. In contrast, U EFs are substantially lower in the Scaglia Bianca Formation, ranging from <1 to ~20, with U EF <3 in all but four samples.

In the Morelos Formation, $\delta^{238}U$ values range from −0.72‰ to

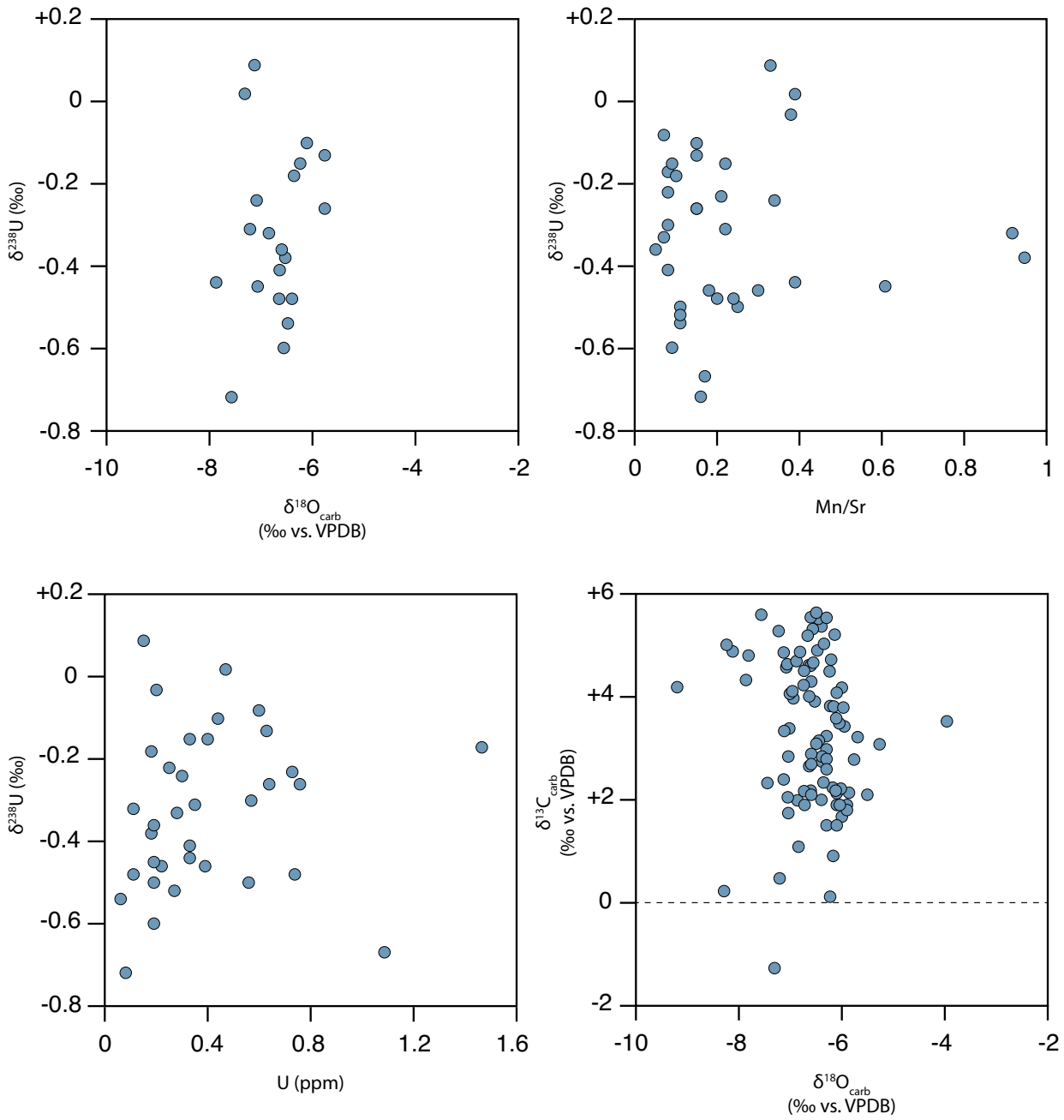

Fig. 4. Scatter plots of important geochemical variables for carbonates of the Morelos Formation. Note the lack of correlation between $\delta^{238}U$ and diagenetic indicators such as $\delta^{18}O$ ($R^2 = 0.02$) and Mn/Sr ratio ($R^2 = 0.00$). $\delta^{238}U$ also does not correlate with U concentration ($R^2 = 0.01$). These data indicate a lack of systematic alteration of $\delta^{238}U$ values. Lastly, there is no covariation between $\delta^{13}C$ and $\delta^{18}O$ ($R^2 = 0.01$), which would be expected if samples were influenced by meteoric diagenesis. Together, these trends give us confidence in the near-primary nature of our $\delta^{238}U$ signal. $\delta^{13}C$ and $\delta^{18}O$ data from Elrick et al. (2009).

+0.09‰ with two discrete negative excursions (Figs. 4, 5). The base of the section records decreasing $\delta^{238}U$ values from near −0.10‰ to −0.50‰, followed by increasing values which peak at +0.09‰ at ~22 m. Through this interval, $\delta^{13}C$ values begin at near +4‰, decrease briefly to values near +2‰, and then increase again to near +4‰. $\delta^{238}U$ values then progressively decrease to a relatively prolonged nadir of near −0.50‰ before increasingly again to values as high as −0.15‰. Through this interval, $\delta^{13}C$ values first show a sharp decrease down to near −1‰, followed by a rapid increase and relatively prolonged zenith near +5‰. There is then a progressive decrease back to +2‰ at the top of the section. Broadly, the interval between ~22 and 62 m defines a clear negative $\delta^{238}U$ excursion that inversely mirrors the positive $\delta^{13}C$ excursion that defines OAE 2, with potential temporal offsets between the $\delta^{238}U$ and $\delta^{13}C$ records discussed below.

Through the Morelos Formation, $\delta^{18}O$ values are relatively invariant near −6‰, with the exception of a discrete interval with values down to −9‰ between 35 and 38 m (Figs. 2, 4). All $\delta^{18}O$ values for the studied BT section (with the exception of two data points) are between −5.9 and − 8.3‰ (Elrick et al., 2009). Manganese to Sr ratios (Mn/Sr)—which are used as a diagenetic indicator—are <1 in all samples (Fig. 4), and Mg/Ca ratios (an index of dolomitization) are <0.04 in all but one sample.

In the Scaglia Bianca Formation, $\delta^{13}C$ values are relatively invariant between +2.0 and +2.5‰ with the exception of a single data point that rises to +2.7‰ at 24 m and two data points that rise to +3.1‰ just above the organic-rich Bonarelli Level that marks OAE 2 (Fig. 3). The higher $\delta^{13}C$ value at 24 m may be related to the mid-Cenomanian Event

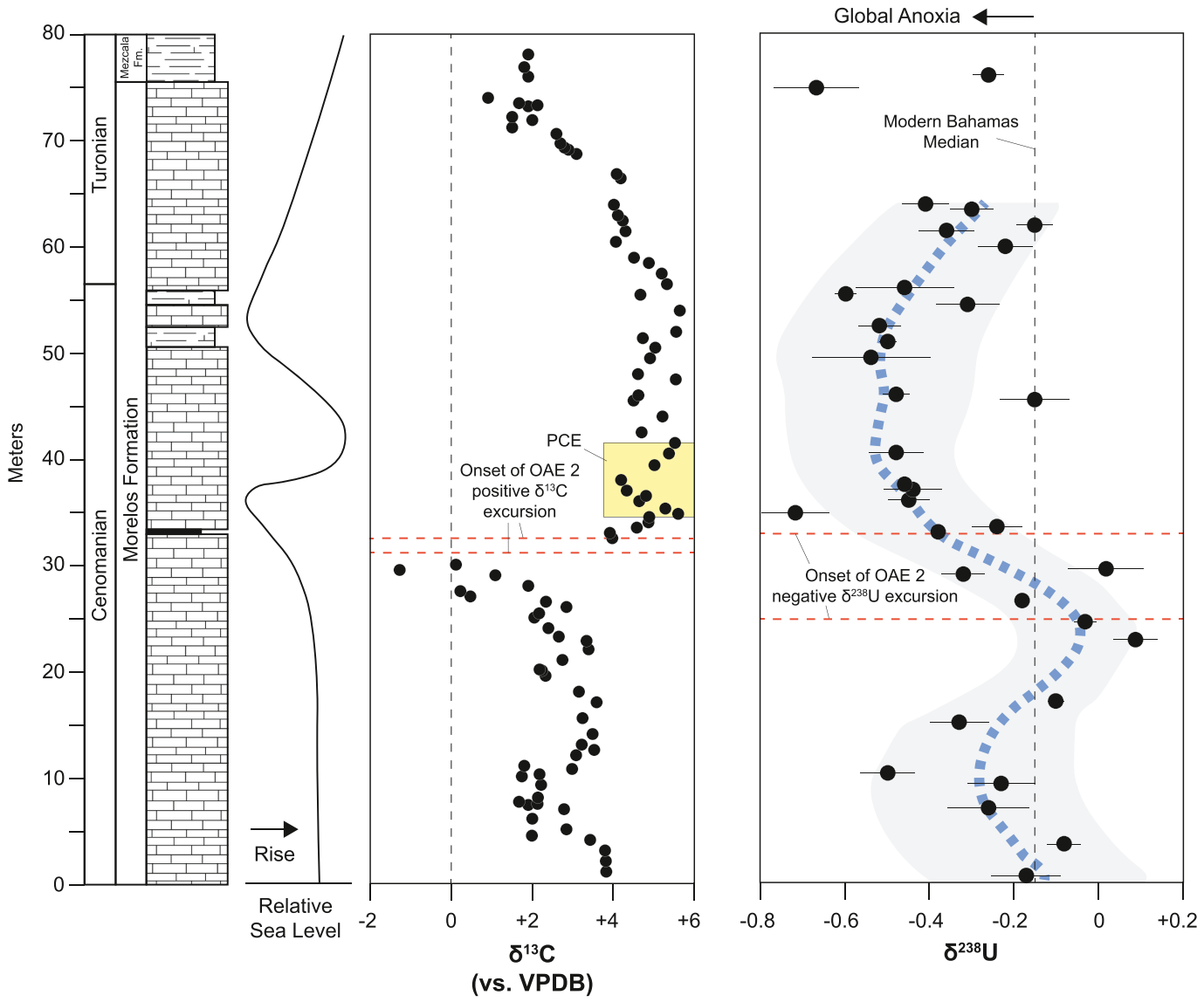

Fig. 5. Stratigraphy, relative sea level curve, and $\delta^{13}C$ and $\delta^{238}U$ trends of the Morelos Formation in the BT section. Left panel: simplified stratigraphy of the section vs. stratigraphic depth (m). Center left panel: relative sea level curve for the BT section (from Elrick et al., 2009). Center right panel: $\delta^{13}C$ vs. stratigraphic depth (from Elrick et al., 2009). Red dashed lines indicate the onset of the positive $\delta^{13}C$ excursion that marks the beginning of OAE 2. Right panel: $\delta^{238}U$ vs. stratigraphic depth. $\delta^{238}U$ error bars are 2 s.d. of replicate measurements. Blue dashed line and grey shaded area is the median and 10,000-member ensemble of LOESS fits (span = 0.489, estimated by the Akaike Information Criterion (AICC)) to the $\delta^{238}U$ data, sampling stratigraphic depth and analytical uncertainties, but excluding the uppermost two points of the section and the positive outlier at 45.5 m ($n = 31$). Red dashed lines indicate upper and lower bound estimates (95th percentile confidence interval) for the onset of the negative $\delta^{238}U$ excursion. PCE = Plenus Cold Event. (For interpretation of the references to colour in this figure legend, the reader is referred to the web version of this article.)

(Coccioni and Galeotti, 2003). In the Scaglia Bianca Formation, $\delta^{18}O$ values exhibit a subtle decreasing stratigraphic trend from −3.0‰ at the base to −4.4‰ at the top (Fig. 3).

5. Discussion

5.1. Diagenesis and detrital influence

We use geochemical and stratigraphic data to evaluate potential depositional and diagenetic influences on $\delta^{238}U$ trends in the Morelos Formation. The dominance of skeletal wackestone and packstone containing abundant benthic body and trace fossils indicates deposition beneath well-oxygenated bottom waters throughout the duration of the section. Carbonates deposited under well-oxygenated conditions have a high potential for recording seawater $\delta^{238}U$ values because of the lack of accumulation of isotopically heavy authigenic U(IV), which could occur if bottom waters or pore waters were anoxic. In addition, relatively smooth stratigraphic changes in $\delta^{238}U$ are recorded in uniform facies through the Morelos Formation (although there is some sample-to-sample variability), arguing against a strongly variable local control on $\delta^{238}U$ values.

Due to differences in the mobility of Sr and Mn, higher Mn/Sr ratios are generated from diagenetic reactions with high fluid/rock ratios and from reducing pore or formation fluids, thus providing a useful monitor of diagenesis (Banner and Hanson, 1990; Jacobsen and Kaufman, 1999). This is because Mn concentrations are low in well-oxygenated seawater but can become enriched in reducing diagenetic fluids, whereas Sr concentrations are high in seawater, but Sr is lost from the carbonate crystal lattice through recrystallization in the presence of non-marine fluids (Banner and Hanson, 1990). Low Mn/Sr ratios (<1) throughout the Morelos Formation thus suggest limited interaction with Mn-rich anoxic porewaters or late-stage burial fluids. $\delta^{18}O$ values largely

Table 1
Summary of localities investigated previously and in this study for $\delta^{238}U$ across Cretaceous OAE 2.

Locality	Geologic Setting	Lithology/Facies	Hydrography	$\delta^{238}U$ pre-OAE 2	OAE 2 $\delta^{238}U$ nadir	OAE 2 $\delta^{238}U$ shift	Notes	Reference
ODP Site 1261A	Demerara Rise, Equatorial Atlantic	Black shale	Open ocean	+0.06 ± 0.06‰	−0.07 ± 0.09‰	~−0.15‰		Montoya-Pino et al. (2010)
Eastbourne	Anglo-Paris Basin, United Kingdom	Alternating marl and pelagic chalk/limestone	Epicontinental sea	~−0.4‰	~−0.7‰	~−0.3‰	Two separate negative $\delta^{238}U$ shifts separated by the Plenus Cold Event	Clarkson et al. (2018)
Raia del Pedale	Southern Apennines, Italy	Fossiliferous limestone	Tethys carbonate platform	~−0.2‰	No clear shift	No clear shift		Clarkson et al. (2018)
South Ferriby	East Midlands Shelf, United Kingdom	Pelagic chalk	Epicontinental sea	~−0.1‰	No clear shift	No clear shift	Unconformity truncates OAE 2	Clarkson et al. (2018)
Portland #1 core	Western Interior Seaway, Colorado, North America	Transition from calcareous grey shale to alternating marl and limestone	Variably restricted epicontinental sea	+0.23 ± 0.06‰	~−1.2‰	~−1.4‰	Magnitude of $\delta^{238}U$ shift corrected to ~ − 0.9‰ based on facies control and variable seawater-sediment fractionation	McDonald et al. (2022)
Morelos Formation	Guerrero-Morelos platform, southern Mexico	Fossiliferous wackestone and packstone	Open Pacific margin carbonate platform	~−0.1‰	~−0.6‰	~−0.5‰		This study

Fig. 6. MCMC inversion results for the Morelos Formation. Solid line denotes median; shading denotes 16th to 84th percentile confidence interval. The large negative U isotope excursion is consistent with an initial expansion of f_{anox} to ~3% and a total interval of expanded euxinia of ~1 Myr. The relative age of each sample was estimated from the sedimentation rates calculated in the text.

between −5.9 and −8.3‰ also argue against diagenetic alteration in the presence of burial fluids with elevated temperatures, with this process commonly resulting in carbonates that are strongly depleted in ^{18}O (Dickson and Coleman, 1990; Hood et al., 2018). There is no statistically significant correlation of $\delta^{238}U$ vs. Mn/Sr, [U], or $\delta^{18}O$ ($R^2 = 0.02$ or less; Fig. 4), indicating a lack of systematic $\delta^{238}U$ alteration, and neither do we find any statistical correlation between $\delta^{13}C$ and $\delta^{18}O$ values of Morelos samples, which would be expected if these platform carbonates were influenced by meteoric diagenesis (Banner and Hanson, 1990; Fig. 4). Because changes in the aragonite content of platform sediment vary with sea-level (with highstand sediments being aragonite-rich and lowstand sediments being calcite-rich; Droxler and Schlager, 1985; Betzler et al., 1999), a eustatic control on sediment uranium isotope compositions would result in correlated $\delta^{238}U$ values and Sr/Ca ratios (with Sr more concentrated in aragonite), as seen in modern Bahamas samples (e.g., Tissot et al., 2018). The weak correlation observed between $\delta^{238}U$ and Sr/Ca ($R^2 = 0.12$) in the Morelos Formation indicates a lack of eustatic control on $\delta^{238}U$. Furthermore, low Mg/Ca ratios (generally <0.04) suggest that dolomitization was minor. It is also important that samples contain sufficient authigenic U from seawater such that its isotopic composition can be discerned above a baseline of detrital U. Uranium EF values of 1 indicate a purely crustal (or detrital) source of U while U EF values >1 indicate authigenic enrichment of U from seawater. All samples from the Morelos Formation are substantially enriched in U above a detrital baseline, with U EF values consistently >20. This suggests that an authigenic seawater $\delta^{238}U$ signal is preserved in these platform strata. In contrast, U EFs in the Scaglia Bianca Formation are consistently <3, indicating substantially less authigenic U from seawater in these pelagic carbonates.

$\delta^{13}C$ trends in the Morelos Formation are similar to those documented in globally distributed Cenomanian-Turonian sections except for the brief negative shift at ~25–30 m occurring just before the main positive excursion. The origin of this shift is unclear, although the lack of perturbation in $\delta^{18}O$ argues against a diagenetic origin (Elrick et al., 2009). There appears to be no overall effect of this feature on $\delta^{238}U$ trends, although we note that the sample with the lowest $\delta^{13}C$ value (BT-29.5) does exhibit an anomalously high $\delta^{238}U$ value that could be related

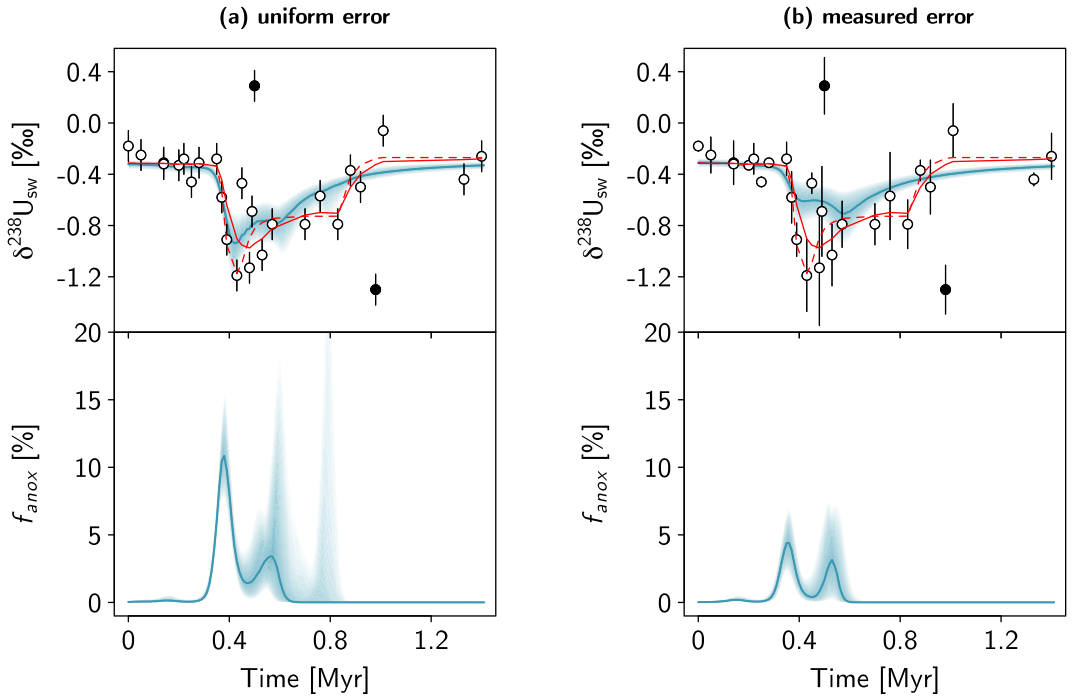

Fig. 7. MCMC inversion results from the Portland core (McDonald et al., 2022). Solid blue lines denote median; shading denotes 16th to 84th percentile confidence interval. Red lines denote model scenarios published in McDonald et al. (2022): dashed and solid lines illustrate, respectively, 70× and 30× increases in anoxia during OAE 2 compared to the modern ocean. Black points are outliers that were removed from inversion. Two scenarios were considered: (A) a uniform error (± 0.12‰) on each estimate of $\delta^{238}U_{SW}$, and (B) the individually-measured error on each $\delta^{238}U_{SW}$ value as reported in McDonald et al. (2022). The uniform error approach better matches the model scenarios of McDonald et al. (2022) because it attempts to fit all points equally; in contrast, the measured-error scenario implies a different f_{anox} trajectory because the most negative points have larger errors. (For interpretation of the references to colour in this figure legend, the reader is referred to the web version of this article.)

to diagenesis. With the exception of this single sample, a steadily decreasing $\delta^{238}U$ shift from ~25 to 35 m is maintained, giving us confidence in the primary origin of this trend. Combined, these relationships suggest that $\delta^{238}U$ trends were not impacted or obscured by local diagenetic or depositional processes.

5.2. Comparison of uranium isotope archives

A negative $\delta^{238}U$ excursion associated with OAE 2 was first recognized by Montoya-Pino et al. (2010) in black shales from mid-Atlantic ODP site 1261A. Additionally, Clarkson et al. (2018) investigated U isotope trends across OAE 2 in pelagic and platform carbonates from Eastbourne (UK), Raia del Pedale (Italy), and South Ferriby (UK). McDonald et al. (2022) also investigated $\delta^{238}U$ in pelagic carbonates from the Western Interior epicontinental seaway (WIS) of North America. Each of these sections record variable $\delta^{238}U$ signals that likely represent a combination of global ocean redox change and local depositional or diagenetic processes (McDonald et al., 2022; Table 1). In black shale of ODP site 1261A, the magnitude of negative $\delta^{238}U$ shift across OAE 2 is ~0.15‰ (Montoya-Pino et al., 2010), whereas the Eastbourne chalk section records two negative $\delta^{238}U$ shifts of ~0.3‰ across the same interval (Clarkson et al., 2018). The Raia del Pedale and South Ferriby sections record generally higher $\delta^{238}U$ values than would be expected for well-preserved carbonates, which Clarkson et al. (2018) attributed to partial recrystallization and dolomitization, and the presence of an unconformity and black shale interval, respectively. It was thus concluded that Eastbourne was the best-preserved section studied by Clarkson et al. (2018), with Raia del Pedale and South Ferriby recording varying degrees of diagenetic overprinting. In pelagic carbonates of the North American WIS, McDonald et al. (2022) reported an ~1.2‰ negative shift in $\delta^{238}U$ across OAE 2, which is substantially greater in magnitude than the other sections discussed above. After considering stratigraphic changes and facies control on the magnitude of fractionation between seawater and sediment, the $\delta^{238}U$ shift across OAE 2 was corrected to ~0.9‰ (McDonald et al., 2022), which is still considerably larger than the shift recorded in Eastbourne (Clarkson et al., 2018) and ODP site 1261A (Montoya-Pino et al., 2010). McDonald et al. (2022) discussed a variety of mechanisms to explain this larger magnitude shift including local U cycling in epeiric seas, with the ~0.9‰ shift occurring at the facies transition from the Hartland Shale to the Bridge Creek Limestone. This facies change corresponded to a sea level rise and ventilation of WIS bottom-waters at the onset of OAE 2, which may have created a flux of oxidized U(VI) into the epeiric watermass from marine sediments originally deposited under anoxic conditions prior to OAE 2. This local effect could have modified the WIS $\delta^{238}U$ record compared to the open ocean, but McDonald et al. (2022) emphasized that the Eastbourne chalk section of Clarkson et al. (2018) also represents an epeiric sea that could have been subject to local U cycling effects. Both the Bridge Creek Limestone (WIS section) and Eastbourne chalk comprise alternating marlstone and limestone, which additionally suggests local variability in facies and redox that could influence $\delta^{238}U$ signals (McDonald et al., 2022).

The strength of the Morelos Formation (analyzed in this study) as a seawater $\delta^{238}U$ archive lies in its deposition on the open Pacific margin away from any epeiric or restricted watermasses (Fig. 1). The consistency of locally well-oxygenated facies (fossiliferous and bioturbated wackestone and packstone) throughout the Morelos Formation also bodes well for the fidelity of the $\delta^{238}U$ signal, which was not impacted by facies changes and variations in local bottom-water oxygenation. In the Morelos Formation, the negative $\delta^{238}U$ shift across OAE 2 is ~0.5‰ (Fig. 5), which is comparable to other OAEs across Phanerozoic time (e.g., the Permo-Triassic and Triassic-Jurassic boundaries; Jost et al., 2017; Zhang et al., 2018). This negative $\delta^{238}U$ shift of ~0.5‰ is intermediate between the shift of ~0.15‰ recorded at ODP site 1261A (Montoya-

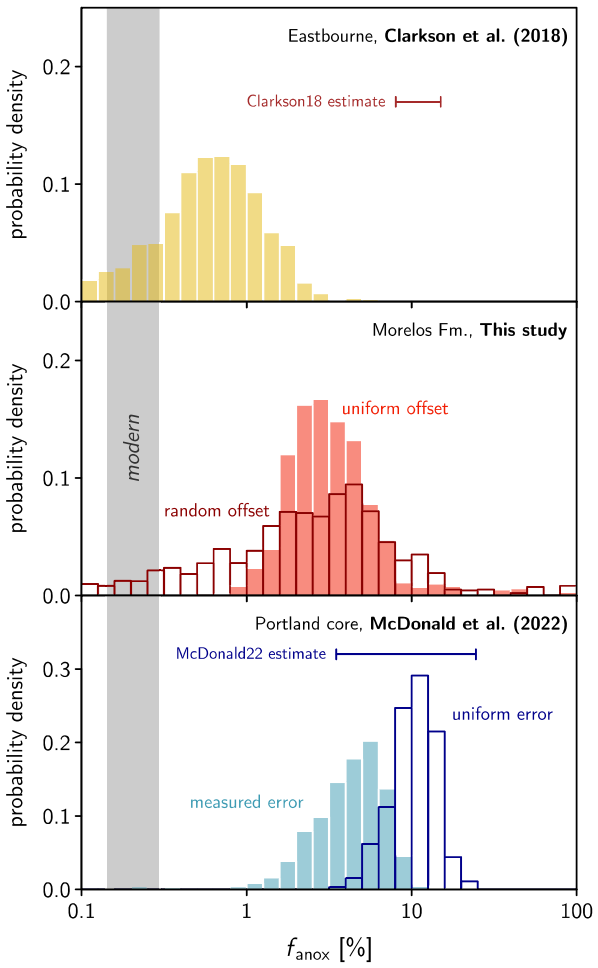

Fig. 8. Histogram of reconstructed anoxic extent at peak onset of OAE 2 from multiple sites. Each histogram represents the anoxic extent at peak onset in 1000 forward model runs sampling the posterior distribution from the MCMC inversion. Data from Clarkson et al. (2018) were modeled in Kipp and Tissot (2022). Data from the Morelos Formation were modeled in this study, under assumptions of a uniform (+0.23‰) and variable (+0.23 ± 0.15‰) offset between $\delta^{238}U_{carb}$ and $\delta^{238}U_{SW}$. Data from the Portland core were generated in McDonald et al. (2022); their inferred $\delta^{238}U_{SW}$ values were modeled here; while the authors of that study considered variable diagenetic offsets in their $\delta^{238}U_{SW}$ reconstruction, we considered two scenarios: uniform error and measured analytical error, which gave rise to different best-fit trends. Grey bar denotes modern anoxic extent. Brackets denote previously-published estimates of f_{anox} from Clarkson et al. (2018) and McDonald et al. (2022). Variability in inferred f_{anox} across sites likely derives from seawater heterogeneity during the transient perturbation and/or from fluctuations in the fidelity of each unit as an archive of $\delta^{238}U_{SW}$.

Pino et al., 2010) and ~0.9‰ recorded in the WIS (McDonald et al., 2022), and most closely matches the Eastbourne chalk section that records an ~0.3‰ negative $\delta^{238}U$ excursion (Clarkson et al., 2018).

Differences between these signals could also result from paleoenvironmental differences between pelagic chalks (such as the Eastbourne section) and platform carbonates rich in benthic fauna such as the Morelos Formation (Elrick et al., 2009). Studies of pelagic carbonates across the mid-Cretaceous, Paleocene-Eocene Thermal Maximum (PETM), and the Holocene of the Indian Ocean found low initial U concentrations in pelagic calcite (Clarkson et al., 2020, 2021; Chen et al., 2022b), substantially lower than U concentrations measured in platform carbonates of the Morelos Formation. These low U concentrations are comparable to our measurements of pelagic carbonates across OAE 2 from the Scaglia Bianca Formation of Italy (median [U] = 0.04 ppm), although higher U concentrations were reported in pelagic carbonates from the WIS across OAE 2 (McDonald et al., 2022). In contrast, platform carbonates have higher initial U concentrations even in original calcite, with this difference potentially reflecting the relative proportion of primary biogenic vs. early diagenetic authigenic carbonate phases, with authigenic phases such as early marine cements containing higher U abundances (Clarkson et al., 2021) and being more prevalent in porous platform carbonates. We suggest that both pelagic and platform carbonates have strengths and weaknesses as seawater $\delta^{238}U$ archives that need to be considered on a case-by-case basis. Pelagic carbonates are subject to less secondary U addition in total, but their low initial U concentrations mean they are poorly buffered against secondary U addition, such that secondary U would have a proportionally larger impact on preserved $\delta^{238}U$ values. In contrast, higher initial U concentrations in platform carbonates could make this archive more robust against diagenetic changes in $\delta^{238}U$, but the presence of U in a variety of phases formed throughout the paragenetic history of the rock (as opposed to most U in pelagic carbonates residing in primary biogenic calcite) potentially makes platform carbonates a more complex $\delta^{238}U$ archive that requires careful diagenetic assessment. Below, we dynamically model $\delta^{238}U$ data from all OAE 2 sections studied to date with sufficient age control to provide quantitative estimates of seafloor anoxic area across OAE 2, thus demonstrating the utility of comparing these different archives.

5.3. Uranium isotopes and global redox trends across OAE 2

At the base of the Morelos Formation section, $\delta^{238}U$ values begin near −0.15‰, which is identical to the median value of modern Bahamian carbonate sediments (Chen et al., 2018; Tissot et al., 2018). This observation suggests initial deposition in oceans with a near-modern degree of oxygenation. A negative $\delta^{238}U$ excursion is then observed at ~10 m, which could be interpreted as a brief pre-OAE 2 expansion of ocean anoxia, although the excursion is strongly defined by one data point with a relatively low $\delta^{238}U$ value of −0.50‰. We thus do not emphasize this potential pre-OAE 2 excursion in the following discussion and modeling exercise. $\delta^{238}U$ values then return to near-modern carbonate values at ~22 m, indicating a return to well-oxygenated oceans. Beginning at ~22 m, a clear negative shift of ~0.5‰ occurs, and $\delta^{238}U$ values remain low (with a minimum of −0.60‰) for ~30 m of section. This pronounced negative $\delta^{238}U$ excursion is interpreted as a major pulse of global marine anoxia that corresponds with OAE 2. $\delta^{238}U$ values then return to near-modern values at the top of the section, indicating that the oceans were ventilated in the OAE 2 aftermath.

Of particular interest is that the main negative $\delta^{238}U$ excursion appears to begin before the positive $\delta^{13}C$ shift that is traditionally used to identify OAE 2. At the studied section, the OAE 2 positive $\delta^{13}C$ excursion starts between 27 and 31 m and ends at 75 m, implying that it spans between 44 and 48 m of section (Fig. 5). To define the onset of the $\delta^{238}U$ excursion, we sampled and propagated stratigraphic depth and analytical uncertainty in $\delta^{238}U$ to create an ensemble of LOESS curves (Fig. 5) and evaluated the results above 20 m in the section. If the onset of the $\delta^{238}U$ excursion is defined as falling below the median value of modern Bahamas carbonates (−0.15‰; Chen et al., 2018; Tissot et al., 2018), then the 95th percentile confidence interval for the depth of onset of the $\delta^{238}U$ excursion is 27 to 33 m (Fig. 5, right panel, upper red dashed line at 33 m). If the onset of the $\delta^{238}U$ excursion is defined as following the maximum of the $\delta^{238}U$ LOESS curve, then the depth of onset of the excursion is 25 to 30 m (Fig. 5, right panel, lower red dashed line at 25 m).

Sageman et al. (2006) estimated the duration of the OAE 2 positive $\delta^{13}C$ excursion as between 847 and 885 kyr. Together with the stratigraphic range of OAE 2 in the Morelos Formation of 44 to 48 m, this implies a minimum mean sedimentation rate of 4.97 cm/kyr and a maximum mean sedimentation rate of 5.66 cm/kyr. For the scenario defining the $\delta^{238}U$ excursion relative to the median modern carbonate $\delta^{238}U$ value, we estimate that the onset of the negative $\delta^{238}U$ excursion

could have been coeval with the onset of the positive $\delta^{13}C$ excursion or it could have preceded the onset of the positive $\delta^{13}C$ excursion by as much as 127 kyr (95th percentile confidence interval). The median estimate spanning uncertainty in the LOESS curve fit is that the onset of the negative $\delta^{238}U$ excursion preceded the onset of the positive $\delta^{13}C$ excursion by 45 to 51 kyr. For the scenario defining the $\delta^{238}U$ excursion relative to the maximum Morelos Formation $\delta^{238}U$ value, we estimate that the onset of the negative $\delta^{238}U$ excursion preceded the onset of the positive $\delta^{13}C$ excursion by 51 to 168 kyr (95th percentile confidence interval), with the median estimate, spanning LOESS curve fit uncertainty, of 105 to 120 kyr. These results indicate that the negative $\delta^{238}U$ excursion is likely to have preceded the positive $\delta^{13}C$ excursion, suggesting a causal relationship whereby the expansion of marine anoxia drove enhanced organic carbon burial. If this is correct, we would expect to see a similar lead-lag relationship between $\delta^{238}U$ and $\delta^{13}C$ in future studies of coeval OAE 2 sections.

Similar lags between $\delta^{238}U$ and $\delta^{13}C$ excursions are recognized in several other Phanerozoic successions, including across the Late Cambrian SPICE event where a negative $\delta^{238}U$ excursion precedes $\delta^{13}C$ increase by ~400 kyr in the astronomically calibrated Alum Shale, Sweden (Zhao et al., 2022, 2023). A similar pattern is also apparent across the onset of the Early Mississippian TICE excursion in Nevada (Cheng et al., 2020) and the Triassic-Jurassic boundary in northern Italy where $\delta^{238}U$ values begin to decrease before the P1 positive $\delta^{13}C$ excursion and reach their nadir before the P2 positive $\delta^{13}C$ excursion (Jost et al., 2017), indicating a delayed oceanographic response between ocean anoxia and organic carbon burial. Marine deoxygenation preceding $\delta^{13}C$ change was also recognized for OAE 2 using thallium isotopes in organic-rich sediments from Demerara Rise, where Ostrander et al. (2017) recognized thallium isotope change ~43 ± 11 kyr before carbon cycle perturbation. This estimate is in good agreement with our $\delta^{238}U$ results from the Morelos Formation, particularly our median estimate of a 45 to 51 kyr offset between $\delta^{238}U$ and $\delta^{13}C$ change based on when $\delta^{238}U$ values fall below modern carbonate values. Owens et al. (2016) also found that seawater vanadium (V) drawdown, which is a response to expanding marine anoxia, preceded the onset of carbon cycle perturbation during OAE 2. These lines of evidence, along with our new $\delta^{238}U$ data, suggest that the expansion of ocean anoxia preceded organic carbon burial, which has been interpreted as the main driver of the positive $\delta^{13}C$ excursion (e.g., Kuypers et al., 2002; Owens et al., 2018; Papadomanolaki et al., 2022). We also note that exact estimates of the temporal offset between the onset of anoxia and $\delta^{13}C$ change would be expected to vary between sections (based on different methods for determining depositional duration in different lithologies) and between different proxies for anoxia (e.g., [Mo], [V], Tl isotopes, and U isotopes) that respond at different redox potentials.

An important observation enabled by these data is that traditional estimates of the length of OAE 2 (as well as other OAEs in the geological record) based on the duration of $\delta^{13}C$ excursions and the thickness of organic-rich facies likely underestimate the duration of widespread ocean anoxia. This observation is also demonstrated by differences in timing between osmium (Os) isotope and $\delta^{13}C$ shifts, with the former recording a longer duration of large igneous province activity than traditional OAE estimates (Turgeon and Creaser, 2008; DuVivier et al., 2014; Sullivan et al., 2020). Based on our above analysis of the onset of the negative $\delta^{238}U$ excursion in the Morelos Formation, our data could indicate that expansive ocean anoxia began as much as ~168 kyr before previous estimates based on the $\delta^{13}C$ record (95th percentile confidence interval). Taking both of our methods for estimating the onset of the negative $\delta^{238}U$ excursion into account, as well as the Sageman et al. (2006) estimate of 847 to 885 kyr for the duration of the $\delta^{13}C$ excursion, our data suggest that widespread seafloor anoxia during OAE 2 lasted between 13 and 20% longer than traditional estimates, implying a total length for OAE 2 of >900 kyr (and potentially >1 Myr).

In the pelagic Eastbourne section (Clarkson et al., 2018), a brief negative $\delta^{13}C$ shift within the overall positive OAE 2 excursion was interpreted as the Plenus Cold Event (PCE), which was a brief cooling episode in the middle of the OAE 2 greenhouse (O'Connor et al., 2020). The PCE is bracketed by two negative $\delta^{238}U$ excursions which were interpreted as two distinct pulses of expanded ocean anoxia during OAE 2 (Clarkson et al., 2018). The brief PCE negative $\delta^{13}C$ excursion is also recognized in the studied Morelos Formation with a ~2‰ decrease at ~35 m. In contrast to the Eastbourne section, the Morelos Formation $\delta^{238}U$ profile does not show any change in ocean redox across the PCE. This is consistent with other published OAE 2 sections (Montoya-Pino et al., 2010; McDonald et al., 2022), which also do not exhibit $\delta^{238}U$ change across the PCE. In the Morelos Formation, $\delta^{238}U$ values remain near −0.4‰ through the PCE, which is between the near-modern carbonate values recorded prior to OAE 2 and the nadir of $\delta^{238}U$ recorded at the peak of OAE 2. One possibility to explain this difference is that oxygenation across the PCE was not a global phenomenon (O'Connor et al., 2020) and had only minimal (or heterogeneous) impact on the global U isotope mass balance. Another possibility is that the $\delta^{238}U$ rise recorded across the PCE in the Eastbourne section is a product of local facies and redox variability, with the PCE interval occurring in the Plenus Marl Formation which could record less-oxygenated local conditions than the underlying Grey Chalk Formation (Tsikos et al., 2004; Jenkyns et al., 2017; McDonald et al., 2022), thus promoting increased uptake of isotopically heavy U(IV) during early diagenesis.

5.4. Modeling constraints on seafloor anoxia

Clarkson et al. (2018) considered the Eastbourne $\delta^{238}U$ data in the context of dynamic forward modeling of C, P, O, and U dynamics, estimating that between 8 and 15% of the global seafloor was covered by anoxic waters during the peak of OAE 2. Kipp and Tissot (2022) revisited this dataset with an inverse model designed to optimize the fit to $\delta^{238}U$ data, finding that a smaller extent of anoxia (0.1–2.0%) was more likely to give rise to the Eastbourne data. The discrepancy between these model results derives from the fact that the forward model outputs in Clarkson et al. (2018) were not explicitly fit to the data; the re-analysis by Kipp and Tissot (2022) provided a better fit to the $\delta^{238}U$ time series and thus provides a more likely extent of seafloor anoxia given the Eastbourne dataset.

Here, we used the model of Kipp and Tissot (2022) to also evaluate the extent of anoxia during OAE 2 using $\delta^{238}U$ data from the Morelos Formation (Fig. 6) and the Portland core (Fig. 7; McDonald et al., 2022). We find that the large negative $\delta^{238}U$ excursion recorded in the Morelos Formation suggests an initial peak anoxic extent of about 1–10% of the seafloor (95% confidence interval), with anoxia persisting for ~1 Myr, potentially reaching an even greater extent later in the event. The most likely extent of anoxia is similar when using uniform or variable diagenetic offsets (Fig. 8B), but the variable offset approach gives a broader confidence interval. The Portland core data (McDonald et al., 2022) also imply two pulses of anoxia, with the first either reaching ~10% (Fig. 7A) or ~5% (Fig. 7B) of the global seafloor depending on the approach used to quantify uncertainty in seawater $\delta^{238}U$ estimates.

We note that while the $\delta^{238}U$ trends at all three OAE 2 sites considered here imply two distinct pulses of anoxia, there is variability in their inferred magnitude (Fig. 8). There are two main reasons for this. The first reason is that, as seen in Figs. 7 and 8, choices about how to best fit the $\delta^{238}U$ time series (correction of diagenetic offset, treatment of uncertainty on each data point) can have substantial impacts on inferred f_{anox} trends. We have thus aimed to be conservative here in considering all possible assumptions that go into these f_{anox} reconstructions. The second reason is that different magnitudes of $\delta^{238}U$ change have been recorded at each site (i.e., a smaller excursion at Eastbourne than in the Morelos Formation, and a smaller excursion in the Morelos Formation than in the Portland core). This could derive from spatially heterogenous $\delta^{238}U$ signals propagating through the ocean as OAE 2 progressed, as well as from different sites varying in their fidelity as archives of the seawater $\delta^{238}U$ value. While future work could disentangle precisely

what mechanisms explain the difference in trends between these sites, this study highlights the importance of utilizing multiple coeval localities to study dynamics of seafloor deoxygenation during OAEs.

6. Conclusions

1) High-resolution $\delta^{13}C$, $\delta^{238}U$, and elemental geochemistry from well-preserved platform carbonates of southern Mexico were used to evaluate seawater redox trends across Cretaceous OAE 2.
2) The $\delta^{238}U$ profile indicates near-modern levels of ocean oxygenation at the base of the section (late Cenomanian), followed by a potential pulse of marine anoxia prior to OAE 2. $\delta^{238}U$ values then briefly return to near-modern carbonate values before a well-defined, stratigraphically coherent negative $\delta^{238}U$ excursion down to −0.60‰ that indicates a major expansion of global ocean anoxia across OAE 2. $\delta^{238}U$ then returns to near-modern carbonate values at the top of the section.
3) The onset of expanded marine anoxia as recorded by the negative $\delta^{238}U$ anomaly precedes the positive $\delta^{13}C$ excursion that marks OAE 2 by a median of ~45 to 51 kyr or ~105 to 120 kyr depending on how the onset of the $\delta^{238}U$ anomaly is estimated. This is consistent with previous thallium isotope and trace metal data (Owens et al., 2016; Ostrander et al., 2017) that also indicate expanded ocean anoxia prior to the onset of carbon cycle perturbation.
4) The temporal relationship between $\delta^{13}C$ and $\delta^{238}U$ trends suggests that the expansion of ocean anoxia related to OAE 2 preceded (and potentially resulted in) expanded organic carbon burial, which is recorded in the globally recognized positive $\delta^{13}C$ excursion.
5) These results suggest that OAE 2 may have lasted >900 kyr, which is longer than traditional estimates. The observation that $\delta^{13}C$ change lags behind ocean anoxia necessitates a reassessment of using $\delta^{13}C$ records to estimate the duration of OAEs in Earth history.
6) The reconstructed peak anoxic seafloor extent of OAE 2 slightly differs when considering the Morelos Formation and Portland core data (1–10%) versus the Eastbourne data (0.1–2%; Clarkson et al., 2018 data reinterpreted by Kipp and Tissot, 2022). This highlights the importance of using multiple sample sites to reconstruct ocean deoxygenation during OAEs, even for global tracers such as uranium, as subtle seawater heterogeneity and differences in local diagenesis can modify global trends.

Declaration of Competing Interest

The authors declare that they have no known competing financial interests or personal relationships that could have appeared to influence the work reported in this paper.

Data availability

All observational data produced in this study are available in the Supplemental Data File as an Excel-format workbook.

Acknowledgements

We thank the American Association of Petroleum Geologists (AAPG) and the George Mason University College of Science for funding this project. FLHT acknowledges support from NSF grant MGG-2054892. AJK acknowledges support from the Fulbright Foundation. We are indebted to Gwyneth Gordon and Trevor Martin for analytical support and Ariel D. Anbar for use of instrumentation at Arizona State University, as well as Richard Ash for analytical support at the University of Maryland. We also thank Linda Hinnov for writing support. Jeremy Owens and an anonymous reviewer are thanked for their helpful and constructive criticisms, and we thank Alex Dickson for editorial handling.

Appendix A. Supplementary data

Supplementary data to this article can be found online at https://doi.org/10.1016/j.palaeo.2023.111756.

References

Adams, D.D., Hurtgen, M.T., Sageman, B.B., 2010. Volcanic triggering of a biogeochemical cascade during Oceanic Anoxic Event 2. Nat. Geosci. 3, 201–204.
Aguilera-Franco, N., Hernandez-Romano, U., 2004. Cenomanian-Turonian facies succession in the Guerrero-Morelos Basin, Southern Mexico. Sediment. Geol. 170, 135–162.
Banner, J.L., Hanson, G.N., 1990. Calculation of simultaneous isotopic and trace element variations during water-rock interaction with applications to carbonate diagenesis. Geochim. Cosmochim. Acta 54, 3123–3137.
Bertine, K.K., Turekian, K.K., 1973. Molybdenum in marine deposits. Geochim. Cosmochim. Acta 37, 1415–1434.
Betzler, C., Reijmer, J.J.G., Bernet, K., Eberli, G.P., Anselmetti, F.S., 1999. Sedimentary patterns and geometries of the Bahamian outer carbonate ramp (Miocene–Lower Pliocene, Great Bahama Bank). Sedimentology 46, 1127–1143.
Bigeleisen, J., 1996. Nuclear size and shape effects in chemical reactions: Isotope chemistry of the heavy elements. J. Am. Chem. Soc. 118, 3676–3680.
Brennecka, G.A., Herrmann, A.D., Algeo, T.J., Anbar, A.D., 2011. Rapid expansion of oceanic anoxia immediately before the end-Permian mass extinction. Proc. Natl. Acad. Sci. 108, 17631–17634.
Brown, S.T., Basu, A., Ding, X., Christensen, J.N., DePaolo, D.J., 2018. Uranium isotope fractionation by abiotic reductive precipitation. Proc. Natl. Acad. Sci. 115, 8688–8693.
Bruggmann, S., Gilleaudeau, G.J., Romaniello, S.J., Severmann, S., Canfield, D.E., Anbar, A.D., Scholz, F., Frei, R., 2022. Uranium isotope cycling on the highly productive peruvian margin. Chem. Geol. 590, 120705.
Charbonnier, G., Boulila, S., Spangenberg, J.E., Adatte, T., Föllmi, K.B., Laskar, J., 2018. Obliquity pacing of the hydrological cycle during Oceanic Anoxic Event 2. Earth Planet. Sci. Lett. 499, 266–277.
Chen, X., Robinson, S.A., Romaniello, S.J., Anbar, A.D., 2022b. 238U/235U in calcite is more susceptible to carbonate diagenesis. Geochim. Cosmochim. Acta 326, 273–287.
Chen, X., Romaniello, S., Herrmann, A., Hardisty, D., Gill, B., Anbar, A., 2018. Diagenetic effects on uranium isotope fractionation in carbonate sediments from the Bahamas. Geochim. Cosmochim. Acta 237, 294–311.
Chen, H., Xu, Z., Bayon, G., Lim, D., Batenburg, S.J., Petrizzo, M.R., Hasegawa, T., Li, T., 2022a. Enhanced hydrological cycle during Oceanic Anoxic Event 2 at southern high latitudes: New insights from IODP Site U1516. Glob. Planet. Chang. 209, 103735.
Cheng, K., Elrick, M., Romaniello, S.J., 2020. Early Mississippian Ocean anoxia triggered organic carbon burial and late Paleozoic cooling: evidence from uranium isotopes recorded in marine limestone. Geology 48, 363–367.
Clarkson, M., Stirling, C., Jenkyns, H., Dickson, A., Porcelli, D., Moy, C., Pogge von Strandmann, P.A.E., Cooke, I.R., Lenton, T., 2018. Uranium isotope evidence for two episodes of deoxygenation during Oceanic Anoxic Event 2. Proc. Natl. Acad. Sci. USA 115, 2918–2923.
Clarkson, M.O., Müsing, K., Andersen, M.B., Vance, D., 2020. Examining pelagic carbonate-rich sediments as an archive for authigenic uranium and molybdenum isotopes using reductive cleaning and leaching experiments. Chem. Geol. 539, 119412.
Clarkson, M.O., Lenton, T.M., Andersen, M.B., Bagard, M.L., Dickson, A.J., Vance, D., 2021. Upper limits on the extent of seafloor anoxia during the PETM from uranium isotopes. Nat. Commun. 12, 399.
Coccioni, R., Galeotti, S., 2003. The mid-Cenomanian Event: prelude to OAE 2. Palaeogeogr. Palaeoclimatol. Palaeoecol. 190, 427–440.
Cole, D.B., Planavsky, N.J., Longley, M., Böning, P., Wilkes, D., Wang, X., Swanner, E.D., Wittkop, C., Loydell, D.K., Busigny, V., Knudsen, A.C., Sperling, E.A., 2020. Uranium isotope fractionation in non-sulfidic anoxic settings and the global uranium isotope mass balance. Glob. Biogeochem. Cycles 34, e2020BG006649.
Dickson, A.J., Jenkyns, H.C., Porcelli, D., van den Boorn, S., Idiz, E., 2016. Basin-scale controls on the molybdenum-isotope composition of seawater during Oceanic Anoxic Event 2 (Late Cretaceous). Geochim. Cosmochim. Acta 178, 291–306.
Dickson, J.A.D., Coleman, M.L., 1990. Changes in carbon and oxygen isotope composition during limestone diagenesis. Carbonate Diagenesis. https://doi.org/10.1002/9781444304510.ch21.
Droxler, A.W., Schlager, W., 1985. Glacial versus interglacial sedimentation rates and turbidite frequency in the Bahamas. Geology 13, 799–802.
DuVivier, A.D.C., Selby, D., Sageman, B.B., Jarvis, I., Gröcke, D.R., Voigt, S., 2014. Marine 187Os/188Os isotope stratigraphy reveals the interaction of volcanism and ocean circulation during Oceanic Anoxic Event 2. Earth Planet. Sci. Lett. 389, 23–33.
Elrick, M., Molina-Garza, R., Duncan, R., Snow, L., 2009. C-isotope stratigraphy and paleoenvironmental changes across OAE 2 (mid-Cretaceous) from shallow-water platform carbonates of southern Mexico. Earth Planet. Sci. 277, 295–306.
Elrick, M., Polyak, V., Algeo, T.J., Romaniello, S., Asmerom, Y., Herrmann, A.D., Anbar, A.D., Zhao, L., Chen, Z., 2017. Global-ocean redox variation during the middle-late Permian through early Triassic based on uranium isotope and Th/U trends of marine carbonates. Geology 45, 163–166.
Elrick, M., Gilleaudeau, G.J., Romaniello, S.J., Algeo, T.J., Morford, J., Sabbatino, M., Goepfert, T.J., Chernyavskiy, P., Cleal, C., Cascales-Miñana, B., 2022. Major Early-Middle Devonian oceanic oxygenation linked to early land plant evolution detected

using high-resolution U isotopes of marine limestones. Earth Planet. Sci. Lett. 581, 117410.
Evans, M.N., Selmer, K.J., Breeden III, B.T., Lopatka, A.S., Plummer, R.E., 2016. Correction algorithm for online continuous flow δ13C and δ18O carbonate and cellulose stable isotope analyses. Geochem. Geophys. Geosyst. 17, 3580–3588.
Gilleaudeau, G., Romaniello, S., Luo, G., Kaufman, A., Zhang, F., Klaebe, R., Kah, L., Azmy, K., Bartley, J., Zheng, W., Knoll, A., Anbar, A., 2019. Uranium isotope evidence for limited euxinia in mid-Proterozoic oceans. Earth Planet. Sci. Lett. 521, 150–157.
Gomes, M.L., Hurtgen, M.T., Sageman, B.B., 2016. Biogeochemical sulfur cycling during cretaceous oceanic anoxic events: a comparison of OAE1a and OAE2. Paleoceaogr. Paleoclimatol. 31, 233–251.
Handoh, I.C., Lenton, T.M., 2003. Periodic mid-cretaceous oceanic anoxic events linked by oscillations of the phosphorus and oxygen biogeochemical cycles. Glob. Biogeochem. Cycles 17. https://doi.org/10.1029/2003GB002039.
Hernandez-Romano, U., Aguilera-Franco, N., Martinez-Medrano, M., Barcelo-Duarte, J., 1997. Guerrero-Morelos Platform drowning at the Cenomanian-Turonian boundary, Huitziltepec area, Guerrero State, southern Mexico. Cretac. Res. 18, 661–686.
Hetzel, A., Böttcher, M.E., Wortmann, U.G., Brumsack, H.J., 2009. Paleo-redox conditions during OAE 2 reflected in Demerara rise sediment geochemistry (ODP Leg 207). Palaeogeogr. Palaeoclimatol. Palaeoecol. 273, 302–328.
Holmden, C., Amini, M., Francois, R., 2015. Uranium isotope fractionation in Saanich Inlet: a modern analog study of a paleoredox tracer. Geochim. Cosmochim. Acta 153.
Hood, A.V.S., Planavsky, N.J., Wallace, M.W., Wang, X., 2018. The effects of diagenesis on geochemical paleoredox proxies in sedimentary carbonates. Geochim. Cosmochim. Acta 232, 265–287.
Jacobsen, S.B., Kaufman, A.J., 1999. The Sr, C and O isotopic evolution of Neoproterozoic seawater. Chemical Geology 161, 37–57.
Jarvis, I., Lignum, J.S., Gröcke, D.R., Jenkyns, H.C., Pearce, M.A., 2011. Black shale deposition, atmospheric CO2 drawdown, and cooling during the Cenomanian-Turonian Oceanic Anoxic Event. Paleoceanogr. Paleoclimatol. 26 https://doi.org/10.1029/2010PA002081.
Jenkyns, H.C., 2010. Geochemistry of oceanic anoxic events. Geochem. Geophys. Geosyst. 11.
Jenkyns, H.C., Dickson, A.J., Ruhl, M., van den Boorn, S.H.J.M., 2017. Basalt-seawater interaction, the Plenus Cold Event, enhanced weathering and geochemical change: deconstructing Oceanic Anoxic Event 2 (Cenomanian–Turonian, late Cretaceous). Sedimentology 64, 16–43.
Jost, A.B., Bachan, A., van de Schootbrugge, B., Lau, K.V., Weaver, K.L., Maher, K., Payne, J.L., 2017. Uranium isotope evidence for an expansion of marine anoxia during the end-Triassic extinction. Geochem. Geophys. Geosyst. 18, 3093–3108.
Kendall, B., 2021. Recent advances in geochemical paleo-oxybarometers. Annu.Rev. Earth Planet. Sci. 49, 399–433.
Kipp, M.A., Tissot, F.L.H., 2022. Inverse methods for consistent quantification of seafloor anoxia using uranium isotope data from marine sediments. Earth Planet. Sci. Lett. 577, 117240.
Kipp, M.A., Li, H., Ellwood, M.J., John, S.G., Middag, R., Adkins, J.F., Tissot, F.L.H., 2022. 238U, 235U and 234U in seawater and deep-sea corals: a high-precision reappraisal. Geochim. Cosmochim. Acta 336, 231–248.
Ku, T.-L., Knauss, K.G., Mathieu, G.G., 1977. Uranium in open ocean: Concentration and isotopic composition. Deep-Sea Res. 24, 1005–1017.
Kuypers, M.M.M., Pancost, R.D., Nijenhuis, I.A., Sinninghe Damsté, J.S., 2002. Enhanced productivity led to increased organic carbon burial in the euxinic North Atlantic basin during the late Cenomanian oceanic anoxic event. Paleoceanogr. Paleoclimatol. 17, 2000PA000569.
Lau, K.V., Maher, K., Altiner, D., Kelley, B.M., Kump, L.R., Lehrmann, D.J., Silva-Tamayo, J.C., Weaver, K.L., Yu, M., Payne, J.L., 2016. Marine anoxia and delayed Earth system recovery after the end-Permian extinction. Proc. Natl. Acad. Sci. 113, 2360–2365.
Lau, K.V., Hancock, L.G., Severmann, S., Kuzminov, A., Cole, D.B., Behl, R.J., Planavsky, N.J., Lyons, T.W., 2022. Variable local basin hydrography and productivity control the uranium isotope paleoredox proxy in anoxic black shales. Geochim. Cosmochim. Acta 317, 433–456.
Lau, K.V., Romaniello, S.J., Zhang, F., 2019. The uranium isotope paleoredox proxy. Cambridge Elements.
Lenniger, M., Nøhr-Hansen, H., Hills, L.V., Bjerrum, C.J., 2014. Arctic black shale formation during cretaceous Oceanic Anoxic Event 2. Geology 42, 799–802.
Lowery, C.M., Cunningham, R., Barrie, C.D., Bralower, T., Snedden, J.W., 2017. The northern Gulf of Mexico during OAE 2 and the relationship between water depth and black shale development. Paleoceanogr. Paleoclimatol. 32 https://doi.org/10.1002/2017PA003180.
McDonald, B.S., Partin, C.A., Sageman, B., Holmden, C., 2022. Uranium isotope reconstruction of ocean deoxygenation during OAE 2 hampered by uncertainties in fractionation factors and local U-cycling. Geochim. Cosmochim. Acta 331, 143–164.
Monteiro, F.M., Pancost, R.D., Ridgwell, A., Donnadieu, Y., 2012. Nutrients as the dominant control on the spread of anoxia and euxinia across the Cenomanian-Turonian oceanic anoxic event (OAE2): Model-data comparison. Paleoceaogr. Paleoclimatol. 27 https://doi.org/10.1029/2012PA002351.
Montoya-Pino, C., Weyer, S., Anbar, A.D., Pross, J., Oschmann, W., van de Schootbrugge, B., Arz, H.W., 2010. Global enhancement of ocean anoxia during Oceanic Anoxic Event 2: a quantitative approach using U isotopes. Geology 38, 315–318.
O'Connor, L.K., Jenkyns, H.C., Robinson, S.A., Remmelzwaal, S.R.C., Batenburg, S.J., Parkinson, I.J., Gale, A.S., 2020. A re-evaluation of the Plenus Cold Event, and links between CO2, temperature, and seawater chemistry during OAE 2. Paleoceanogr. Paleoclimatol. 35, e2019PA003631.
Ostrander, C.M., Owens, J.D., Nielsen, S.G., 2017. Constraining the rate of oceanic deoxygenation leading up to a cretaceous Oceanic Anoxic Event (OAE-2: ~94 Ma). Sci. Adv. 3 https://doi.org/10.1126/sciadv.1701020.
Owens, J.D., Gill, B.C., Jenkyns, H.C., Lyons, T.W., 2013. Sulfur isotopes track the global extent and dynamics of euxinia during Cretaceous Oceanic Anoxic Event 2. Proc. Natl. Acad. Sci. 110, 18407–18412.
Owens, J.D., Lyons, T.W., Lowery, C.M., 2018. Quantifying the missing sink for global organic carbon burial during a cretaceous oceanic anoxic event. Earth Planet. Sci. Lett. 299, 83–94.
Owens, J.D., Reinhard, C.T., Rohrssen, M., Love, G.D., Lyons, T.W., 2016. Empirical links between trace metal cycling and marine microbial ecology during a large perturbation to Earth's carbon cycle. Earth Planet. Sci. Lett. 449, 407–417.
Owens, S.A., Buessler, K.O., Sims, K.W.W., 2011. Re-evaluating the 238U-salinity relationship in seawater: Implications for the 238U–234Th disequilibrium method. Mar. Chem. 127, 31–39.
Papadomanolaki, N.M., van Helmond, N.A.G.M., Pälike, H., Sluijs, A., Slomp, C.P., 2022. Quantifying volcanism and organic carbon burial across Oceanic Anoxic Event 2. Geology 50, 511–515.
Pogge von Strandmann, P.A.E., Jenkyns, H.C., Woodfine, R.G., 2013. Lithium isotope evidence for enhanced weathering during Oceanic Anoxic Event 2. Nat. Geosci. 6, 668–672.
Raven, M.R., Fike, D.A., Bradley, A.S., Gomes, M.L., Owens, J.D., Webb, S.A., 2019. Paired organic matter and pyrite δ34S records reveal mechanisms of carbon, sulfur, and iron cycle disruption during Ocean Anoxic Event 2. Earth Planet. Sci. Lett. 512, 27–38.
Robinson, L.J., George, K.S., Fox, C.P., Marshall, J.E.A., Harding, I.C., Bown, P.R., Lively, J.R., Marroquin, S., Leckie, R.M., Dameron, S., Gröcke, D.R., Papadomanolaki, N.M., van Helmond, N.A.G.M., Whiteside, J.H., 2023. Redox conditions and ecological resilience during Oceanic Anoxic Event 2 in the Western Interior Seaway. Palaeogeogr. Palaeoclimatol. Palaeoecol. 618, 111496.
Rolison, J.M., Stirling, C.H., Middag, R., Rijkenberg, M.J.A., 2017. Uranium stable isotope fractionation in the Black Sea: Modern calibration of the 238U/235U paleo-redox proxy. Geochim. Cosmochim. Acta 203, 69–88.
Romaniello, S.J., Herrmann, A.D., Anbar, A.D., 2013. Uranium concentrations and 238U/235U isotope ratios in modern carbonates from the Bahamas: assessing a novel paleoredox proxy. Chem. Geol. 362, 305–316.
Rudnick, R.L., Gao, S., 2003. The composition of the continental crust. In: Holland, H.D., Turekian, K.K. (Eds.), Treatise on Geochemistry 3. The Crust, Elsevier-Pergamon, Oxford, pp. 1–64.
Sageman, B.B., Meyers, S.R., Arthur, M.A., 2006. Orbital time scale and new C-isotope record for Cenomanian-Turonian boundary stratotype. Geology 34, 125–128.
Scotese, C.R., 2014. Atlas of Late Cretaceous Paleogeographic Maps, PALEOMAP Atlas for ArcGIS, volume 2, The Cretaceous, Maps 16 – 22, Mollweide Projection. PALEOMAP Project, Evanston, IL.
Sullivan, D.L., Brandon, A.D., Eldrett, J., Bergman, S.C., Wright, S., Minisini, D., 2020. High resolution osmium data record three distinct pulses of magmatic activity during cretaceous Oceanic Anoxic Event 2 (OAE-2). Geochim. Cosmochim. Acta 285, 257–273.
Takashima, R., Nishi, H., Huber, B.T., Leckie, E.M., 2006. Greenhouse world and the Mesozoic Ocean. Oceanography 19, 82–92.
Tissot, F.L.H., Dauphas, N., 2015. Uranium isotopic compositions of the crust and ocean: Age corrections, U budget and global extent of modern anoxia. Geochim. Cosmochim. Acta 167, 113–143.
Tissot, F.L.H., Chen, C., Go, B., Naziemiec, M., Healy, G., Bekker, A., Swart, P., Dauphas, N., 2018. Controls of eustasy and diagenesis on the 238U/235U of carbonates and evolution of the seawater (234U/238U) during the last 1.4 Myr. Geochim. Cosmochim. Acta 242, 233–265.
Trabucho Alexandre, J., Tuenter, E., Henstra, G.A., Can der Zwan, K.J., van de Wal, R.S.W., Dijkstra, H.A., de Boer, P.L., 2010. The mid-Cretaceous North Atlantic nutrient trap: Black shales and OAEs. Paleoceanogr. Paleoclimatol. 25.
Tsikos, H., Jenkyns, H.C., Walsworth-Bell, B., Petrizzo, M.R., Forster, A., Kolonic, S., Erba, E., Premoli Silva, I., Baas, M., Wagner, T., Sinninghe DamstÉ, J.S., 2004. Carbon-isotope stratigraphy recorded by the Cenomanian-Turonian Oceanic Anoxic Event: correlation and implications based on three key localities. J. Geol. Soc. 161, 711–719.
Turgeon, S.C., Creaser, R.A., 2008. Cretaceous oceanic anoxic event 2 triggered by a massive magmatic episode. Nature 454, 323–326.
Uchman, A., Rodriguez-Tovar, F.J., Machaniec, E., Kedzierski, M., 2013. Ichnological characteristics of late cretaceous hemipelagic and pelagic sediments in a submarine high around the OAE-2 event: a case from the Rybie section, Polish Carpathians. Palaeogeogr. Palaeoclimatol. Palaeoecol. 370, 222–231.
Veeh, H.H., 1967. Deposition of uranium from the ocean. Earth Planet. Sci. Lett. 3, 145–150.
Vergbruggen, H.H., Alonso, A., Eykens, R., Kehoe, F., Kuhn, H., Richter, S., Aregbe, Y., 2008. Preparation and certification of IRMM-3636. IRMM-3636a and IRMM-3636b.
Westermann, S., Vance, D., Cameron, V., Archer, C., Robinson, S.A., 2014. Heterogeneous oxygenation states in the Atlantic and Tethys oceans during Oceanic Anoxic Event 2. Earth Planet. Sci. Lett. 404, 178–189.
Weyer, S., Anbar, A.D., Gerdes, A., Gordon, G.W., Algeo, T.J., Boyle, E.A., 2008. Natural fractionation of 238U/235U. Geochim. Cosmochim. Acta 72, 345–359.
Zhang, F., Algeo, T.J., Romaniello, S.J., Cui, Y., Zhao, L., Chen, Z.-Q., Anbar, A.D., 2018. Congruent Permian-Triassic δ238U records at Panthalassic and Tethyan sites: confirmation of global-oceanic anoxia and validation of the U-isotope paleoredox proxy. Geology 46, 327–330.
Zhang, F., Lenton, T., Alvaro, R., Romaniello, S., Chen, X., Planavsky, N., Clarkson, M., Dahl, T., Lau, K., Wang, W., Li, Z., Zhao, M., Isson, T., Algeo, T., Anbar, A., 2020.

Uranium isotopes in marine carbonates as a global ocean paleoredox proxy: a critical review. Geochim. Cosmochim. Acta 287, 27–49.
Zhao, Z., Pang, X., Zou, C., Dickson, A.J., Basu, A., Guo, Z., Pan, S., Nielsen, A.T., Schovsbo, N.H., Jing, Z., Dahl, T.W., 2023. Dynamic oceanic redox conditions across the late Cambrian SPICE event constrained by molybdenum and uranium isotopes. Earth Planet. Sci. Lett. 604, 118013.
Zhao, Z., Thibault, N.R., Dahl, T.W., Schovsbo, N.H., Sørensen, A.L., Rasmussen, C.M.Ø., Nielsen, A.T., 2022. Synchronizing rock clocks in the late Cambrian. Nat. Commun. 13, 73–87.